Effects of 2,6-Dichlorophenyl Substituents on the Coordination Chemistry of Pyridine Dipyrrolide Iron Complexes

Brett M. Hakey,^[a] Dylan C. Leary,^[a] Jose G. Rodriguez,^[a] Jordan C. Martinez,^[a] Nicholas B. Vaughan,^[a] Jonathan M. Darmon,^[b] Novruz G. Akhmedov,^[a] Jeffrey L. Petersen,^[a] Brian S. Dolinar,^[a] and Carsten Milsmann*^[a]

A series of iron complexes featuring the pyridine dipyrrolide (PDP) pincer ligand [CI2PhPDPPh]2-, obtained via deprotonation of 2,6-bis(5-(2,6-dichlorophenyl)-3-phenyl-1H-pyrrol-2-yl)pyridine, $H_2^{CI2Ph}PDP^{Ph}$, is reported and structurally and spectroscopically characterized. While the bis-pyridine adduct (CI2PhPDPPh)Fe(py)₂ exhibits nearly identical features as previously reported (MesPDPPh)Fe(py)₂ ($H_2^{Mes}PDP^{Ph}=2,6$ -bis(5-(2,4,6-trimethylphenyl)-3-phenyl-1H-pyrrol-2-yl)pyridine), the diethyl ether and tetrahydrofuran adducts (CI2PhPDPPh)Fe(OEt₂) and (CI2PhPDPPh)Fe(thf) show additional weak Fe—CI interactions that impact the overall coordination geometries and result in strong deviations from planar coordination environments. The reaction of (CI2PhDPPPh)

Fe(thf) with 1-adamantyl azide provided the isolable iron imido complex (Cl2PhPDPPh)Fe(N¹Ad), highlighting the improved stability of [Cl2PhPDPPh]2- towards intramolecular nitrene group transfer from the high-valent iron-imido unit. The electronic structure of (Cl2PhPDPPh)Fe(N¹Ad) was investigated by density functional theory (DFT) and complete active space self-consistent field (CASSCF) calculations. These computational studies suggest energetically close-lying diamagnetic and paramagnetic states and help to conceptualize the unusual magnetic properties of the complex observed by variable-temperature ¹H NMR spectroscopy.

Introduction

Pincer-type pyridine dipyrrolide (PDP) ligands are developing into a versatile platform for the synthesis of transition metal complexes and main group compounds with intriguing electronic structures and reactivity. Following initial work by Caulton and coworkers exploring the coordination chemistry of late transition metal PDP complexes, (PDP)M(L) (M=Pd, Pt, and Zn),^[1] Dash and coworkers recently reported the successful application of palladium PDP complexes as catalysts in tandem Heck alkynylation/cyclization reactions.^[2] At the other extreme of the d-block elements, we have demonstrated the remarkable photophysical properties of zirconium bis-PDP complexes, Zr(PDP)₂, that enabled the design of rare early transition metal photosensitizers operating via excited states with ligand-to-metal charge transfer character.^[3-6] These photoluminescent complexes can replace and, in some cases, outperform tradi-

tional precious metal chromophores as photocatalysts in organic photoredox reactions. Furthermore, studies using the isostructural group 6 complexes $[M(PDP)_2]^{n-}$ (M=Cr and Mo; n = 2-, 1-, 0) unambiguously established the redox-active nature of PDP ligands.^[7]

The excellent tunability of the steric and electronic environments provided by the PDP framework has also inspired detailed studies of transition metal and main group compounds with unusual electronic configurations and coordination environments. Turner characterized the first main group PDP compounds using magnesium, antimony, and bismuth and showed that a rare Bi^{II} species supported by a PDP ligand can be transiently generated and chemically trapped. [8] An even clearer picture for the range of interesting electronic structures stabilized by different PDP ligands is emerging for iron and cobalt complexes. Using a highly sterically encumbered PDP derivative with 3,5-di-tert-butyl-substituted pyrrolide units, [tBuPDPtBu]2-, Mindiola and coworkers were able to isolate the remarkably stable iron(IV)-imido complex (tBuPDPtBu)Fe(N1Ad).[9] Due to the particular steric profile of the pincer ligand that blocks coordination trans to the pyridine unit of the pincer, the complex exhibits an unusual cis-divacant octahedral coordination environment around the iron center that results in a diamagnetic low-spin d⁴ ground state. In addition to imido formation upon exposure to organic azides, the Fe^{II} starting material (tBuPDPtBu)Fe(OEt2) can engage in small molecule activation while retaining cis-divacant octahedral geometries in the corresponding products. This is exemplified by its reaction with elemental sulfur^[10] and formation of a dinuclear bridging dinitrogen complex upon reduction with KC₈.^[11] Similar cis-

N. B. Vaughan, N. G. Akhmedov, J. L. Petersen, B. S. Dolinar,

C. Milsmann

C. Eugene Bennett Department of Chemistry, West Virginia University, Morgantown, West Virginia, USA

E-mail: camilsmann@mail.wvu.edu

[b] J. M. Darmon

Department of Chemistry,

Princeton University,

Princeton, New Jersey, USA

Supporting information for this article is available on the WWW under https://doi.org/10.1002/zaac.202100117

[[]a] B. M. Hakey, D. C. Leary, J. G. Rodriguez, J. C. Martinez,

divacant octahedral geometries were established in cobalt chemistry for (tBuPDPtBu)Co(OEt₂) and the isolable organic azide adduct (tBuPDPtBu)Co(N₃1Ad). The latter undergoes rapid intramolecular nitrene insertion into a C–H bond of a *tert*-butyl substituent upon irradiation with a Xe light source.

By changing the PDP pyrrolide substituents from tert-butyl to aryl groups, we have recently been able to access iron PDP square-planar and complexes with square-pyramidal geometries. [13,14] Most notably, the π -donor properties of the PDP ligand framework favor high-spin configurations of the iron center and allowed for the isolation of rare square-planar high-spin Fe^{II} complexes.^[13] Treatment of (MesPDPPh)Fe(OEt₂) or (MesPDPPh)Fe(thf) with organic azides resulted in a broad range of reactivity depending on the organic substituent of the azide, including formation of iron tetrazene complexes and intramolecular C-H activation by nitrene insertion into the benzylic C-H bonds of the PDP mesityl substituents.[14] While these reactions were proposed to proceed through paramagnetic iron imido or nitrene intermediates, the high reactivity of these putative species prohibited their observation or isolation.

Based on our previous studies, one major obstacle to extending the observed C-H amination reactivity of (MesPDPPh) Fe complexes to intermolecular chemistry relevant to catalytic hydrocarbon functionalization is the presence of weak benzylic C-H bonds in the [MesPDPPh]2- ligand scaffold. To eliminate the possibility for competing intramolecular reactivity while maintaining the overall geometric features of the ligand, the studies presented herein detail our efforts to synthesize iron complexes containing the more robust ligand [CI2PhPDPPh]2-. By replacing the mesityl substituents in [MesPDPPh]2- with sterically similar 2,6dichlorophenyl groups, we were able to restore synthetic access to isolable iron imido complexes. Notably, the close proximity of the chloro substituents to the iron center in the (Cl2PhPDPPh)Fe unit renders them chemically non-innocent by allowing for weak Fe-Cl interactions. These donor interactions significantly impact the overall geometry and electronic structure of the resulting complexes in the solid state.

Results and Discussion

Synthesis and characterization of $H_2^{Cl2Ph}PDP^{Ph}$. The straightforward synthesis of the ligand precursor 2,6-bis(5-(2,6-dichlorophenyl)-3-phenyl-1*H*-pyrrol-2-yl)-pyridine, $H_2^{Cl2Ph}PDP^{Ph}$, was accomplished following a modification of the two-step procedure reported previously for $H_2^{Mes}PDP^{Ph}$. Stetter reaction between 2,6-pyridinedicarboxaldehyde and two equivalents of the chalcone derivative 1-(2,6-dichlorophenyl)-3-phenyl-2-propen-1-one resulted in formation of the desired 2,6-bis(1,4-dicarbonyl) pyridine intermediate in 75% yield (Scheme 1). Following common Paal-Knorr pyrrole synthesis conditions using ammonium acetate in glacial acetic acid as an ammonia source, $H_2^{Cl2Ph}PDP^{Ph}$ was obtained in 50% yield over two steps.

In addition to characterization by 1H and ^{13}C $\{^1H\}$ NMR spectroscopy in DMSO- d_6 , the solid-state structure of $H_2^{CL2Ph}PDP^{Ph}\cdot DMSO$ was determined by single-crystal X-ray diffraction analysis following recrystallization from a concen-

H
N
H
$$+ 2$$
 $+ 2$
 $+ 2$
 $+ 2$
 $+ 2$
 $+ 3$
 $+ 4$
 $+ 4$
 $+ 4$
 $+ 4$
 $+ 4$
 $+ 4$
 $+ 4$
 $+ 4$
 $+ 4$
 $+ 4$
 $+ 4$
 $+ 4$
 $+ 4$
 $+ 4$
 $+ 4$
 $+ 4$
 $+ 4$
 $+ 4$
 $+ 4$
 $+ 4$
 $+ 4$
 $+ 4$
 $+ 4$
 $+ 4$
 $+ 4$
 $+ 4$
 $+ 4$
 $+ 4$
 $+ 4$
 $+ 4$
 $+ 4$
 $+ 4$
 $+ 4$
 $+ 4$
 $+ 4$
 $+ 4$
 $+ 4$
 $+ 4$
 $+ 4$
 $+ 4$
 $+ 4$
 $+ 4$
 $+ 4$
 $+ 4$
 $+ 4$
 $+ 4$
 $+ 4$
 $+ 4$
 $+ 4$
 $+ 4$
 $+ 4$
 $+ 4$
 $+ 4$
 $+ 4$
 $+ 4$
 $+ 4$
 $+ 4$
 $+ 4$
 $+ 4$
 $+ 4$
 $+ 4$
 $+ 4$
 $+ 4$
 $+ 4$
 $+ 4$
 $+ 4$
 $+ 4$
 $+ 4$
 $+ 4$
 $+ 4$
 $+ 4$
 $+ 4$
 $+ 4$
 $+ 4$
 $+ 4$
 $+ 4$
 $+ 4$
 $+ 4$
 $+ 4$
 $+ 4$
 $+ 4$
 $+ 4$
 $+ 4$
 $+ 4$
 $+ 4$
 $+ 4$
 $+ 4$
 $+ 4$
 $+ 4$
 $+ 4$
 $+ 4$
 $+ 4$
 $+ 4$
 $+ 4$
 $+ 4$
 $+ 4$
 $+ 4$
 $+ 4$
 $+ 4$
 $+ 4$
 $+ 4$
 $+ 4$
 $+ 4$
 $+ 4$
 $+ 4$
 $+ 4$
 $+ 4$
 $+ 4$
 $+ 4$
 $+ 4$
 $+ 4$
 $+ 4$
 $+ 4$
 $+ 4$
 $+ 4$
 $+ 4$
 $+ 4$
 $+ 4$
 $+ 4$
 $+ 4$
 $+ 4$
 $+ 4$
 $+ 4$
 $+ 4$
 $+ 4$
 $+ 4$
 $+ 4$
 $+ 4$
 $+ 4$
 $+ 4$
 $+ 4$
 $+ 4$
 $+ 4$
 $+ 4$
 $+ 4$
 $+ 4$
 $+ 4$
 $+ 4$
 $+ 4$
 $+ 4$
 $+ 4$
 $+ 4$
 $+ 4$
 $+ 4$
 $+ 4$
 $+ 4$
 $+ 4$
 $+ 4$
 $+ 4$
 $+ 4$
 $+ 4$
 $+ 4$
 $+ 4$
 $+ 4$
 $+ 4$
 $+ 4$
 $+ 4$
 $+ 4$
 $+ 4$
 $+ 4$
 $+ 4$
 $+ 4$
 $+ 4$
 $+ 4$
 $+ 4$
 $+ 4$
 $+ 4$
 $+ 4$
 $+ 4$
 $+ 4$
 $+ 4$
 $+ 4$
 $+ 4$
 $+ 4$
 $+ 4$
 $+ 4$
 $+ 4$
 $+ 4$
 $+ 4$
 $+ 4$
 $+ 4$
 $+ 4$
 $+ 4$
 $+ 4$
 $+ 4$
 $+ 4$
 $+ 4$
 $+ 4$
 $+ 4$
 $+ 4$
 $+ 4$
 $+ 4$
 $+ 4$
 $+ 4$
 $+ 4$
 $+ 4$
 $+ 4$
 $+ 4$
 $+ 4$
 $+ 4$
 $+ 4$
 $+ 4$
 $+ 4$
 $+ 4$
 $+ 4$
 $+ 4$
 $+ 4$
 $+ 4$
 $+ 4$
 $+ 4$
 $+ 4$
 $+ 4$
 $+ 4$
 $+ 4$
 $+ 4$
 $+ 4$
 $+ 4$
 $+ 4$
 $+ 4$
 $+ 4$
 $+ 4$
 $+ 4$
 $+ 4$
 $+ 4$
 $+ 4$
 $+ 4$
 $+ 4$
 $+ 4$
 $+ 4$
 $+ 4$
 $+ 4$
 $+ 4$
 $+ 4$
 $+ 4$
 $+ 4$
 $+ 4$
 $+ 4$
 $+ 4$
 $+ 4$
 $+ 4$
 $+ 4$
 $+ 4$
 $+ 4$
 $+ 4$
 $+ 4$
 $+ 4$
 $+ 4$
 $+ 4$
 $+ 4$
 $+ 4$
 $+ 4$
 $+ 4$
 $+ 4$
 $+ 4$
 $+ 4$
 $+ 4$
 $+ 4$
 $+ 4$
 $+ 4$
 $+ 4$
 $+ 4$
 $+ 4$
 $+ 4$
 $+ 4$
 $+ 4$
 $+ 4$
 $+ 4$
 $+ 4$
 $+ 4$
 $+ 4$
 $+ 4$
 $+ 4$
 $+ 4$
 $+ 4$
 $+ 4$
 $+ 4$
 $+ 4$
 $+ 4$
 $+ 4$
 $+ 4$
 $+ 4$
 $+ 4$
 $+ 4$
 $+ 4$
 $+ 4$
 $+ 4$
 $+ 4$
 $+ 4$
 $+ 4$
 $+ 4$
 $+ 4$
 $+ 4$
 $+ 4$
 $+ 4$
 $+ 4$
 $+ 4$
 $+ 4$
 $+ 4$
 $+ 4$
 $+ 4$
 $+ 4$
 $+ 4$
 $+ 4$
 $+ 4$
 $+ 4$
 $+ 4$
 $+ 4$
 $+ 4$
 $+ 4$
 $+ 4$
 $+ 4$
 $+ 4$
 $+ 4$
 $+ 4$
 $+ 4$
 $+ 4$
 $+ 4$
 $+ 4$
 $+ 4$
 $+ 4$
 $+ 4$
 $+ 4$
 $+ 4$
 $+ 4$
 $+ 4$
 $+ 4$
 $+ 4$
 $+ 4$
 $+ 4$
 $+ 4$
 $+ 4$
 $+ 4$
 $+ 4$
 $+ 4$

Scheme 1. Synthesis of H₂^{Cl2Ph}PDP^{Ph}.

Scheme 2. Synthesis of (Cl2PhPDPPh)Fe(py)₂.

trated DMSO solution of the compound. A representation of the molecular structure is shown in Figure 1 and highlights the tight hydrogen bonding interaction between the two N–H protons of the pyrrole moieties and the oxygen atom of a DMSO molecule.

Synthesis and characterization of (Cl2PhPDPPh)FeL_n complexes. To determine similarities between the coordination behavior of [Cl2PhPDPPh]²⁻ and previously reported [MesPDPPh]²⁻, the formation of Fe^{II} complexes utilizing the novel chlorinated ligand was explored. Direct treatment of a toluene solution of Fe(Ns)₂py₂ (Ns=CH₂SiMe₃; py=pyridine), containing two neosilyl groups as internal bases, with one equivalent of H₂Cl2PhPDPPh resulted in precipitation of an orange solid identified as (Cl2PhPDPPh)Fe(py)₂ in 56% yield as an analytically pure powder. Recrystallization by slow evaporation of a concentrated dichloromethane solution of (Cl2PhPDPPh)Fe(py)₂ provided single

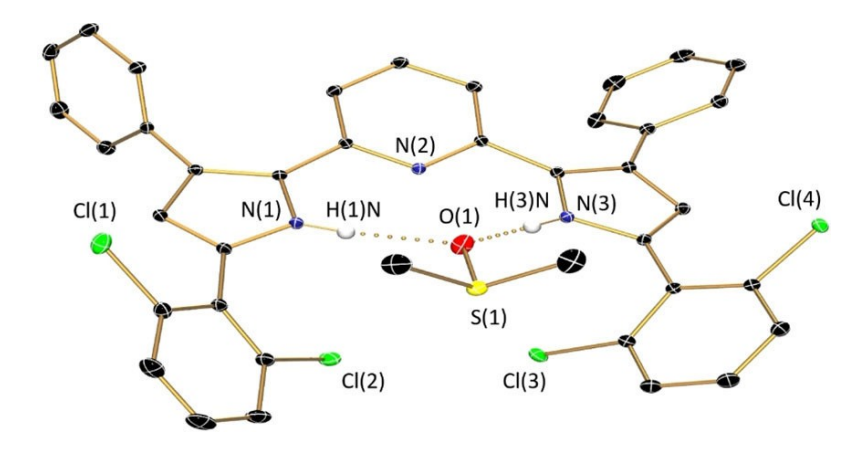


Figure 1. Molecular structure of H₂^{Cl2Ph}PDP^{Ph} shown with 30% probability ellipsoids obtained by X-ray diffraction analysis. Hydrogen atoms except for the pyrrole hydrogens are omitted for clarity.

crystals suitable for X-ray crystallography. An ORTEP representation of the molecular structure is shown in Figure 2.

The structure of (Cl2PhPDPPh)Fe(py)2 is almost identical to that previously reported for (MesPDPPh)Fe(py)2 and contains an iron center in a square-pyramidal coordination environment. Importantly, the 2,6-dichlorophenyl substituents are oriented in nearperpendicular orientation to the plane of the PDP π -system with dihedral angles of 118.8° and 104.8°, supporting a similar steric profile as the mesityl substituents in (MesPDPPh)Fe(py)2 (dihedral angles: 120.9° and 110.2°). All Fe-N bonds are significantly longer than 2 Å, in agreement with a high-spin configuration at iron (Table 1). The Fe-N bonds in the basal positions for (CI2PhPDPPh)Fe(py)2 are very similar compared to those in (MesPDPPh)Fe(py)2. A more pronounced difference can be observed for the pyridine ligand in the apical position. One complication in accurately determining the Fe(1)-N(5) bond length is the presence of disorder in the crystal structure of (CI2PhPDPPh)Fe(py)2. Refinement of the atom position for the apical pyridine required a model with two distinct orientations reflecting a wagging motion of the two pyridine ligands with respect to the pincer ligand. This motion is also reflected in the large thermal ellipsoids for the second pyridine ligand, which indicate less pronounced, and therefore unresolved, disorder. With this caveat in mind, the bond lengths for the apical pyridine ligand, Fe(1)-N(5)A and Fe(1)-N(5)B, were determined to be 2.033(13) Å and 2.113(3) Å, respectively. These bond distances are substantially shorter than that of the apical Fe-N bond in (MesPDPPh)Fe(py)2 at 2.165(1) Å and indicate a stronger metal ligand interaction.

The ¹H NMR spectrum of (^{Cl2Ph}PDP^{Ph})Fe(py)₂ exhibits 11 paramagnetically shifted and broadened resonances consistent with apparent C_{2v} symmetry in solution. This is in stark contrast with the C_s symmetric structure observed in the solid state and indicates that the two pyridine ligands can interchange their basal and apical positions via a wagging vibration. The spectroscopic equivalence of the protons of both pyridine ligands indicates that the dynamic of the wagging motion is fast on the NMR time scale in solution. This is further supported

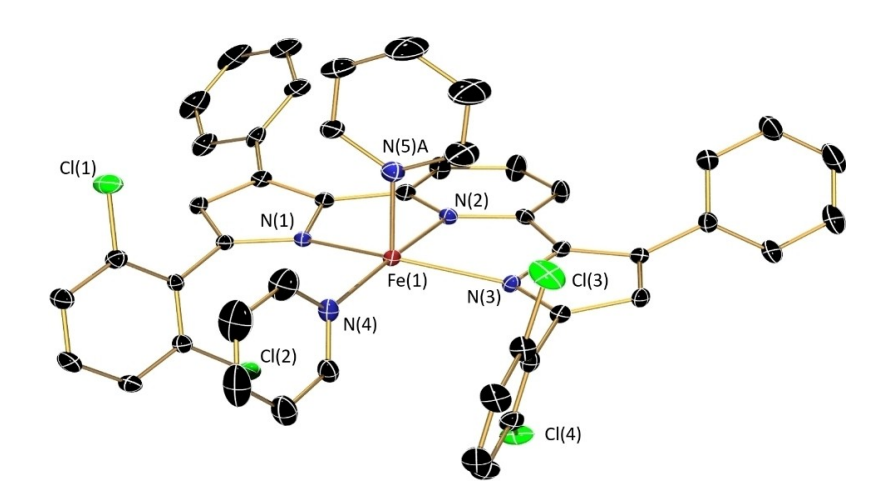


Figure 2. Representation of the molecular structure of (Cl2PhPDPPh)Fe(py)₂ obtained by X-ray diffraction analysis shown with 30% probability ellipsoids. Only one position for the disordered apical pyridine ligand is depicted. Hydrogen atoms are omitted for clarity.

| $[Fe] = (^{Cl2Ph}PDP^{Ph})Fe$ | [Fe](py) ₂ | [Fe](OEt ₂) | [Fe](thf) | [Fe](thf) ₂ | [Fe](N ¹ Ad) |
|-------------------------------|-----------------------|-------------------------|------------|------------------------|-------------------------|
| Fe(1)-N(1) | 2.072(3) | 2.065(3) | 2.0732(15) | 2.097(4) | 1.887(4) |
| Fe(1)-N(2) | 2.074(3) | 2.099(3) | 2.0749(14) | 2.098(4) | 1.898(4) |
| Fe(1)-N(3) | 2.076(3) | 2.045(3) | 2.0599(14) | 2.110(4) | 1.894(4) |
| Fe(1)-N(4) | 2.116(3) | _ | _ | _ | 1.620(4) |
| Fe(1)-N(5) ^a | 2.113(3) | _ | _ | _ | _ |
| | 2.033(13) | | | | |
| Fe(1)-O(1) | _ | 2.091(3) | 2.0555(13) | 2.117(3) | _ |
| Fe(1)-O(2) | _ | _ | _ | 2.177(3) | _ |
| Fe(1)-Cl ^b | no interaction | 2.6324(11) | 2.7161(5) | no interaction | 3.289 |

by a single resonance for the *meta*-protons on the 2,6-dichlorophenyl substituents.

Solid-state magnetic susceptibility measurements at room temperature provided an effective magnetic moment, μ_{eff} , of 4.7 μ_B consistent with a high-spin Fe II configuration. This was further confirmed by 57 Fe Mössbauer spectroscopy, recorded at 80 K on a powder sample of $(^{\text{Cl2Ph}}\text{PDP}^{\text{Ph}})\text{Fe}(\text{py})_2$, which provided a single quadrupole doublet with an isomer shift, δ , of 0.99 mm s $^{-1}$ and an absolute quadrupole splitting, $|\Delta E_Q|$, of 3.12 mm s $^{-1}$ (Figure S14). The combination of a high isomer shift and large quadrupole splitting is characteristic for high-spin Fe II centers with square-pyramidal geometries. The nearly identical Mössbauer parameters for $(^{\text{Cl2Ph}}\text{PDP}^{\text{Ph}})\text{Fe}(\text{py})_2$ and $(^{\text{Mes}}\text{PDP}^{\text{Ph}})$ Fe(py) $_2$ ($\delta=0.98$ mm s $^{-1}$; $|\Delta E_Q|=2.92$ mm s $^{-1}$) further establish similar electronic structures for both compounds.

Having established the structural similarities between the bispyridine iron complexes of [Cl2PhPDPPh]2- and [MesPDPPh]2-, the synthesis of more reactive (Cl2PhPDPPh)Fe complexes was targeted (Scheme 3). Addition of one equivalent of H₂^{Cl2Ph}PDP^{Ph} to a diethylether solution of Fe[N(SiMe₃)₂]₂ resulted in the isolation of red crystals identified as (Cl2PhPDPPh)Fe(OEt2). The molecular structure obtained by X-ray crystallography (Figure 3) establishes a high-spin configuration for the Fe center based on the relatively long Fe-N and Fe-O bonds (> 2.0 Å), which are similar to those in (CI2PhPDPPh)Fe(py)2 and the previously reported, closely related complex (MesPDPPh)Fe(OEt2). However, the geometric parameters of (CI2PhPDPPh)Fe(OEt2) show distinct differences from the structure of (MesPDPPh)Fe(OEt2). While the latter is best described as containing an iron center in a distorted square-planar coordination environment provided by the pincer ligand and a diethyl ether ligand in trans-position to the pyridine ring $(N_{py}\text{-Fe-O} = 160.54(15)^{\circ})$, the ether ligand in (Cl2PhPDPPh)Fe(OEt₂) is substantially lifted out of the (PDP)Fe chelate plane with a N(2)-Fe(1)-O(1) angle of 127.89(11)°. This change in geometry is facilitated by an additional interaction between the iron center and one of the chlorine substituents of a 2,6-dichlorophenyl group (Fe(1)-Cl(1) = 2.632(1) Å), resulting in an overall distorted trigonal-bipyramidal coordination sphere around the iron center. While interactions between organochlorine moieties and metal centers are not uncommon, to the best of our knowledge only two crystallographically characterized examples have been reported for iron. [15,16] A brief survey of the Cambridge Structural Database returned 175 examples of complexes containing short contacts between d- and f-block elements and the chlorine atom of an organochlorine fragment. Many of these examples feature interactions with solvent molecules (dichloromethane or chloroform), but restricting the search further to include only Fe-Cl contacts between first row transition metals and aryl chlorides returned 20 published structures. The M-Cl distances in these complexes extend from 2.30 Å to 3.09 Å, [15-23] indicating that the Fe-Cl interaction in (CI2PhPDPPh)Fe(OEt₂) falls right in the center of this range. The only reported examples for iron exhibit Fe-Cl distances of 2.31 Å¹⁵ and 2.73 Å.^[16]

A very similar structure including short Fe—CI contacts was determined for the corresponding THF adduct, (C12PhPDPPh) Fe(thf), which was isolated following the reaction of FeCl₂ with *in-situ* prepared Li₂(C12PhPDPPh) in THF and subsequent workup using toluene and pentane (Scheme 4). Similar to the previously reported synthesis of (MesPDPPh)Fe(thf), non-polar hydrocarbon solvents were essential to removing the LiCl byproduct formed in the reaction. Single crystals of (C12PhPDPPh)Fe(thf) were obtained via slow diffusion of pentane into a concentrated solution of the complex in benzene, and the molecular structure is shown in Figure 3. Like (C12PhPDPPh)Fe(OEt₂), the solid state structure of (C12PhPDPPh)Fe(thf) exhibits a distorted trigonal-

Scheme 3. Synthesis of $(^{Cl2Ph}PDP^{Ph})Fe(OEt_2)$.

Scheme 4. Synthesis of (Cl2PhPDPPh)Fe(thf).

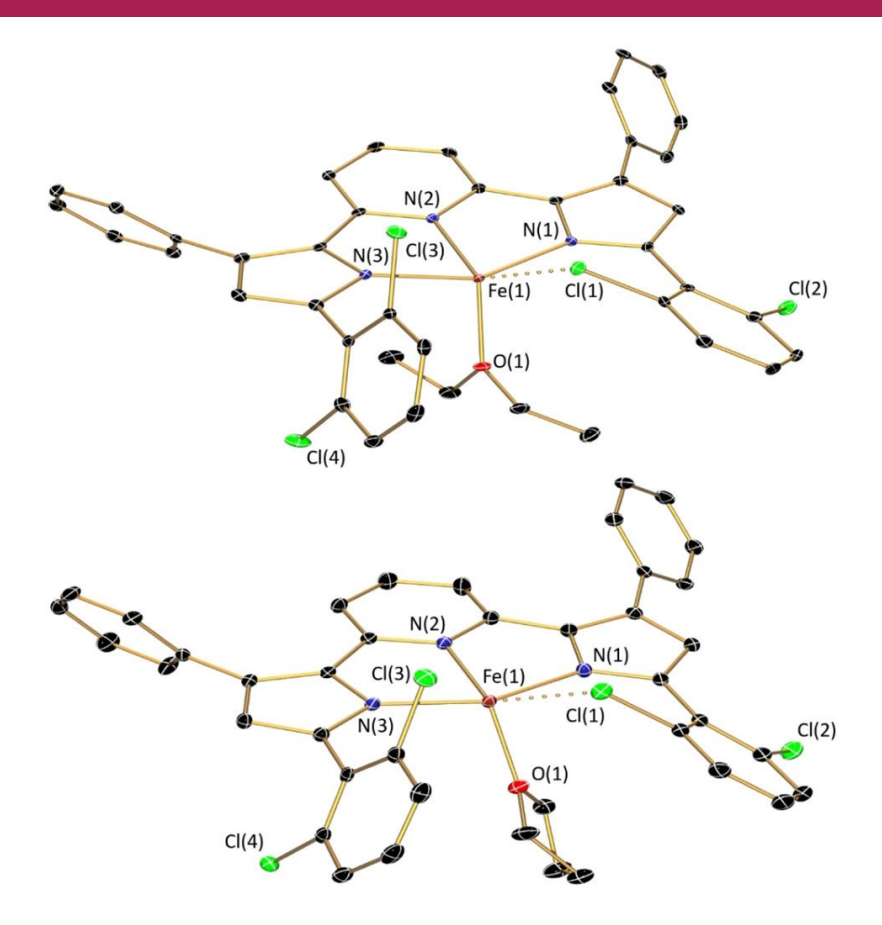


Figure 3. Representations of the molecular structures of (Cl2PhPDPPh)Fe(OEt₂) (top) and (Cl2PhPDPPh)Fe(thf) (bottom) obtained by X-ray diffraction analysis shown with 30% probability ellipsoids. Hydrogen atoms are omitted for clarity.

bipyramidal geometry with a short Fe(1)-Cl(1) contact of 2.7161(5) Å. Consistent with the slightly longer Fe-Cl distance, the N(2)-Fe(1)-O(1) angle of 135.32(6)° is more obtuse than in $(^{Cl2Ph}PDP^{Ph})Fe(OEt_2).$

The additional coordination of a chloro substituent in the solid state is also reflected in the Mössbauer spectroscopic data (Figure 4). While square-planar (MesPDPPh)Fe(thf) exhibits a large isomer shift paired with a small quadrupole splitting (δ =

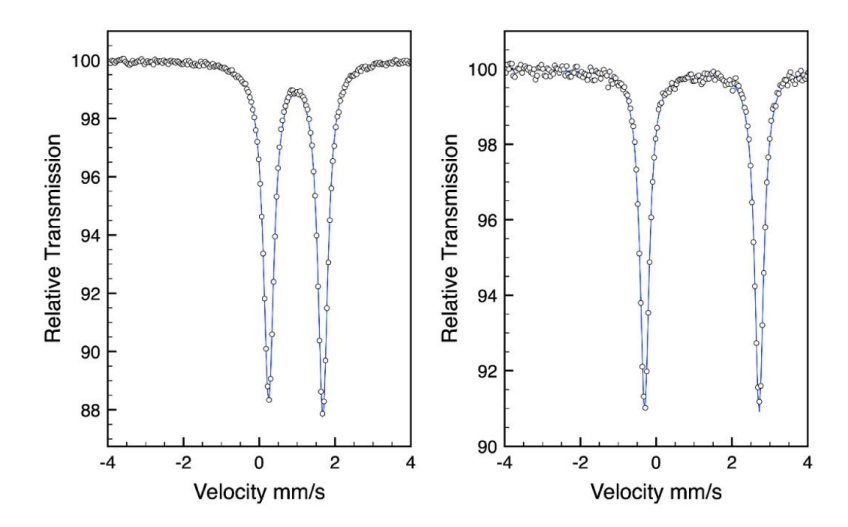


Figure 4. Comparison of the ⁵⁷Fe Mössbauer spectra of solid (CI2PhPDPPh)Fe(thf), (left) and a frozen THF solution of (CI2PhPDPPh)Fe(thf), (right) recorded at 80 K, highlighting the spectral changes upon coordination of an additional THF ligand.

0.78 mm s $^{-1}$, $|\Delta E_Q|=0.48$ mm s $^{-1}$) characteristic for high-spin Fe $^{\rm II}$ complexes in this coordination geometry, $^{[24-26]}$ ($^{(\text{CI2Ph}PDP^{Ph})}$) Fe(thf) shows markedly different spectral features with $\delta=0.96$ mm s $^{-1}$ and $|\Delta E_Q|=1.43$ mm s $^{-1}$. In particular, the significantly increased quadrupole splitting is consistent with a nonplanar molecular structure in which the THF ligand is lifted out of the (PDP)Fe plane. Consequently, the Mössbauer spectroscopic parameters for ($^{\text{CI2Ph}}PDP^{\text{Ph}}$)Fe(thf) more closely resemble the values reported for cis-divacant octahedral ($^{\text{IBu}}PDP^{\text{IBu}}$) Fe(OEt₂) ($\delta=0.86$ mm s $^{-1}$, $|\Delta E_Q|=1.12$ mm s $^{-1}$).

Despite its C_1 -symmetric structure in the solid state, the 1H NMR spectrum of ($^{Cl2Ph}PDP^{Ph}$)Fe(thf) recorded in benzene- d_6 is consistent with apparent C_{2v} symmetry in solution, indicating either that the Fe-Cl interaction is completely absent under these conditions or that all chloride substituents engage interchangeably in Fe-Cl interactions under fast equilibrium conditions on the NMR timescale. Notably, the resonance for the 4-pyridine proton is observed in the upfield region at 0.36 ppm at room temperature. Based on previous studies, [9,13] downfield and upfield shifts of the 4-pyridine proton of PDP ligands compared to the free ligand values are characteristic of high-spin Fe^{II} complexes with and without ligands in cisposition to the PDP pyridine ring, respectively. For reference, square-planar (MesPDPPh)Fe(thf) exhibits a room temperature value of -5.98 ppm for the 4-pyridine proton^[13] while *cis*divacant octahedral (tBuPDPtBu)Fe(OEt2) shows the same resonance at 24.73 ppm.^[9] This can be rationalized by a change of electronic ground-state configuration $(d_{xz})^2(d_{xy})^1(d_{xz})^1(d_{z^2})^1(d_{x^2}-_{y^2})^1$ $(d_{z^2})^2(d_{xz})^1(d_{xy})^1(d_{x^2}-_{y^2})^1$ to upon binding of a ligand in cis-position to the PDP pyridine, which modulates the internal magnetic field experienced by the 4-pyridine proton. Based on these considerations, ¹H NMR spectroscopy indicates a square-planar structure without Fe-Cl interactions for (CI2PhPDPPh)Fe(thf) in solution. However, a more detailed comparison with (MesPDPPh)Fe(thf) establishes that the 4-pyridine proton resonance in (CI2PhPDPPh)Fe(thf) is shifted slightly less upfield, suggesting a limited degree of chlorine interaction and more pronounced deviation from distorted square-planar geometry for (CL2PhPDPPh)Fe(thf) even in solution.

Like its $[^{Mes}PDP^{Ph}]^{2-}$ analog, $(^{Cl2Ph}PDP^{Ph})Fe(thf)$ is capable of binding an additional THF ligand in the apical position to form (CI2PhPDPPh)Fe(thf)₂ as is clearly reflected in substantial changes to the ¹H NMR resonances for solutions of the complex in THF d_8 compared to those observed in benzene- d_6 . Again most indicative, the resonance for the 4-pyridine proton in (Cl2PhPDPPh) Fe(thf)₂ undergoes a downfield shift (22.14 ppm at 25 °C) consistent with the ground state change discussed above. As in the bis-pyridine adduct, (CI2PhPDPPh)Fe(py)2, the number of resonances for $(^{Cl2Ph}PDP^{Ph})Fe(thf)_2$ in THF- d_8 is consistent with apparent C_{2v} symmetry and identical THF ligands on the NMR timescale. Notably, the integrations for the protons of the THF ligands are substantially reduced, indicating facile ligand exchange with THF-d₈. As shown previously for (MesPDPPh) Fe(thf)₂, the coordination of a second THF ligand in (Cl2PhPDPPh) Fe(thf)₂ also has a substantial effect on the Mössbauer spectroscopic parameters (Figure 4), resulting in increases in both isomer shift ($\delta = 1.20 \text{ mm s}^{-1}$) and quadrupole splitting (| $\Delta E_Q \, | =$ 3.02 mm s $^{-1}$) compared to ($^{\text{Cl2Ph}}\text{PDP}^{\text{Ph}}$)Fe(thf).

In contrast to its [MesPDPPh]²⁻ analog that could only be observed spectroscopically in THF solution, single crystals of (CI2PhPDPPh)Fe(thf)₂ were obtained following recrystallization from THF/diethylether. The increased stability of the five-coordinate species with a supporting [CI2PhPDPPh]²⁻ ligand is consistent with the increased bond strength for ligands in the apical position established through structural comparison of otherwise structurally similar (CI2PhPDPPh)Fe(py)₂ and (MesPDPPh)Fe(py)₂ (vide supra). The molecular structure of (CI2PhPDPPh)Fe(thf)₂ obtained via single-crystal X-ray diffraction (Figure 5 and Table 1) confirmed the expected square-pyramidal geometry similar to that of (CI2PhPDPPh)Fe(py)₂.

Reactivity of (C12PhPDPPh)Fe(thf) with 1-adamantyl azide. With well-characterized (C12PhPDPPh)Fe^{III}L_n complexes in hand, we proceeded to test our central hypothesis that the [C12PhPDPPh]²-framework provides a more robust alternative to [MesPDPPh]²- in reactions of the corresponding Fe^{III} complexes with organic azides. Treatment of a dark red dichloromethane solution of (C12PhPDPPh)Fe(thf) with a slight excess of 1-adamantyl azide, N_3^1 Ad, at 40 °C resulted in a color change of the solution to dark

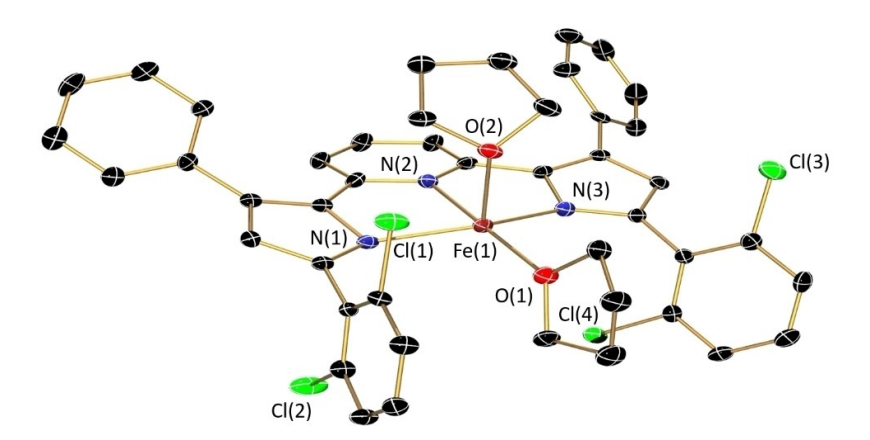


Figure 5. Representation of the molecular structure of (Cl2PhPDPPh)Fe(thf)₂ obtained by X-ray diffraction analysis shown with 30% probability ellipsoids. Hydrogen atoms are omitted for clarity.

brown (Scheme 5). Analysis by ¹H NMR spectroscopy confirmed the formation of a single diamagnetic product with complete consumption of the iron starting material after 4 h. This result is in marked contrast to the same reaction for (MesPDPPh)Fe(thf), which provides the paramagnetic complex (NH1Ad-MesPDPPh) Fe(thf), resulting from nitrene insertion into a benzylic C-H bond of one of the mesityl substituents, as the major product. Addition of excess pentane to the reaction mixture resulted in precipitation of a dark brown solid. Subsequent recrystallization of the crude material via slow evaporation of a diethyl ether solution afforded red-brown single crystals that allowed the identification of the product as the imido complex (Cl2PhPDPPh) Fe(N¹Ad).

A representation of the molecular structure is shown in Figure 6, and the Fe-N bond lengths are summarized in Table 1. Considering only the nitrogen donors, the solid-state structure of (Cl2PhPDPPh)Fe(N1Ad) is reminiscent of the cis-divacant octahedral geometry of the related complex (tBuPDPtBu)Fe(N1Ad) reported by Mindiola and coworkers, with similar Fe-N_{imido} bond lengths of 1.623(4) Å and 1.640(4) Å for the iron-imido fragments, respectively, and very short Fe-N_{pincer} distances $(1.888(3) \text{ Å} - 1.897(3) \text{ Å for } (^{Cl2Ph}PDP^{Ph})Fe(N^1Ad), 1.867(3) \text{ Å} -$ 1.910(2) Å for (tBuPDPtBu)Fe(N1Ad)). These bond lengths are consistent with a low-spin configuration for the iron center under the cryogenic conditions (100 K) used during the X-ray diffraction experiment. As a slight difference between the two imido species, the N_{py} -Fe- N_{imido} angle of 123.06(16) $^{\circ}$ in (CI2PhPDPPh)Fe(N1Ad) is slightly larger than the same angle in (tBuPDPtBu)Fe(N1Ad) at 116.6(2)°, resulting in a more distorted cis-

Scheme 5. Reactivity of (Cl2PhPDPPh)Fe(thf) with 1-adamantyl azide.

divacant octahedral structure. Additionally, one of the chlorine substituents of the 2,6-dichlorophenyl groups exhibits a significantly shortened Fe(1)-Cl(2) distance of 3.289 Å. While this Fe-Cl distance is longer than those observed in other first row transition metal complexes and the solid-state structures of (Cl2PhPDPPh)Fe(thf) and (Cl2PhPDPPh)Fe(OEt₂), it raised the question whether the unusual cis-divacant octahedral structures and the resulting diamagnetic ground states of (PDP)Fe(N¹Ad) complexes are imposed by steric interactions of the imido fragment with the pincer ligand or enforced by electronic preference of the iron center. The former would be consistent with our observations comparing the bent geometries of (CI2PhPDPPh) Fe(thf)/(OEt₂) with their much more planar [MesPDPPh]²⁻ congeners (vide supra) and DFT calculations that show that the lowest energy configuration for (PDP)Fe imido complexes in the absence of steric effects from the PDP ligand is an S=1 state with a distorted square-planar geometry. 14 In contrast, the latter was proposed by Mindiola and coworkers following DFT calculations that showed that the S=0 configuration favors a bent geometry.9

Further motivation to investigate the correlation between the electronic ground state configuration and the geometric features of (CI2PhPDPPh)Fe(N1Ad) was provided by Mössbauer and NMR spectroscopy. The Mössbauer parameters obtained at 80 K using a solid sample of ($^{Cl2Ph}PDP^{Ph}$)Fe(N¹Ad) (δ =-0.08 mm s⁻¹ and $|\Delta E_0| = 2.76 \text{ mm s}^{-1}$, Figure S15) are identical within experimental error to those reported for ($^{tBu}PDP^{tBu}$)Fe(N 1Ad) (δ = -0.09 mm s^{-1} and $|\Delta E_0| = 2.78 \text{ mm s}^{-1}$), suggesting similar electronic ground states with low-spin Fe^{IV} centers and dianionic imido ligands. However, a closer analysis of the NMR spectroscopic data for (Cl2PhPDPPh)Fe(N1Ad) revealed a more complicated pattern. The number of resonances in the ¹H NMR spectrum recorded in dichloromethane- d_2 at room temperature indicates effective C_{2v} symmetry of the complex on the NMR timescale. This is most clearly reflected in the magnetic equivalency of the protons in the meta-position of the 2,6dichlorophenyl substituents, which give rise to a single doublet. The high symmetry observed in solution is inconsistent with

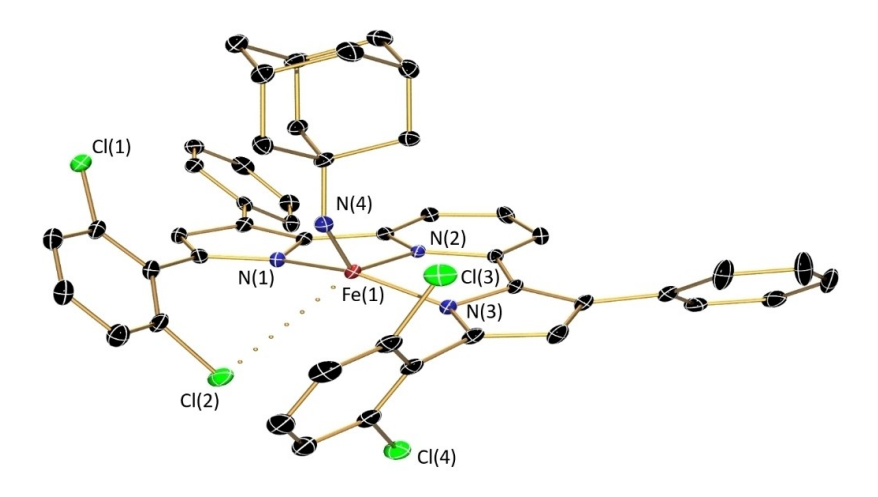


Figure 6. Representation of the molecular structure of (CI2PhPDPPh)Fe(N1Ad) obtained by X-ray diffraction analysis shown with 30% probability ellipsoids. Hydrogen atoms are omitted for clarity. The dotted line indicates the short Fe(1)-Cl(2) interaction of 3.289 Å.

the C_1 -symmetric molecular structure observed in the solid state. Even assuming a fast equilibrium of interchanging chlorine interactions or the absence of these weak interactions in solution, the symmetry for a *cis*-divacant octahedral structure should be C_s . Based on these considerations, the most likely explanation for the apparent C_{2v} symmetry of the complex in solution is a dynamic equilibrium between several lower symmetry structures due to either restricted rotation of the 2,6-dichlorophenyl substituents or a wagging motion of the imido fragment similar to the one proposed for $(^{Cl2Ph}PDP^{Ph})Fe(py)_2$ and $(^{Cl2Ph}PDP^{Ph})Fe(thf)_2$. In the latter case, the N^1Ad ligand changes its position with respect to the π -system of the pincer ligand via a transition state with a square-planar coordination environment around the iron center.

Variable-temperature (VT-)NMR data were collected over a range of $-85\,^{\circ}\text{C}$ to $+45\,^{\circ}\text{C}$ to obtain further insight into the proposed dynamics (Figure 7). Below $-40\,^{\circ}\text{C}$, the resonances for the protons on the 2,6-dichlorophenyl substituents broaden substantially compared to all remaining signals, indicating a slowing of the dynamic process that renders the *meta*-protons magnetically equivalent at elevated temperatures. Unfortunately, the broadening of all spectral features below $-80\,^{\circ}\text{C}$ due to increased viscosity of the solvent prevented the unambig-

uous observation of well-defined signals for magnetically independent meta-2,6-dichlorophenyl protons in a C_s symmetric conformation. While these experiments clearly support the hypothesis of an equilibrium between multiple C_s -symmetric structures in solution, the exact nature of the dynamic process remains unclear.

Even more interestingly, the VT-NMR experiments exposed interesting magnetic properties of (Cl2PhPDPPh)Fe(N1Ad). While the general appearance of the ¹H NMR resonances with wellresolved J-coupling and chemical shifts between 0-8 ppm is expected for a molecule with a diamagnetic ground state, the exact chemical shifts of several signals are unusual. Most notably, the resonance for the pyrrole protons is found at 5.12 ppm at room temperature, substantially further upfield than in other diamagnetic PDP species. Additionally, the resonance for the equivalent 3- and 5-pyridine protons is located at 7.65 ppm. While this chemical shift seems unremarkable for aromatic protons, it is unusual given that the pyridine protons are located within the shielding cone of the flanking phenyl substituents, which should cause a significant upfield shift. This is nicely illustrated by the position of the 4-pyridine resonance, which is located just below 6 ppm in the room temperature spectrum. Finally, the signals for the adamantyl

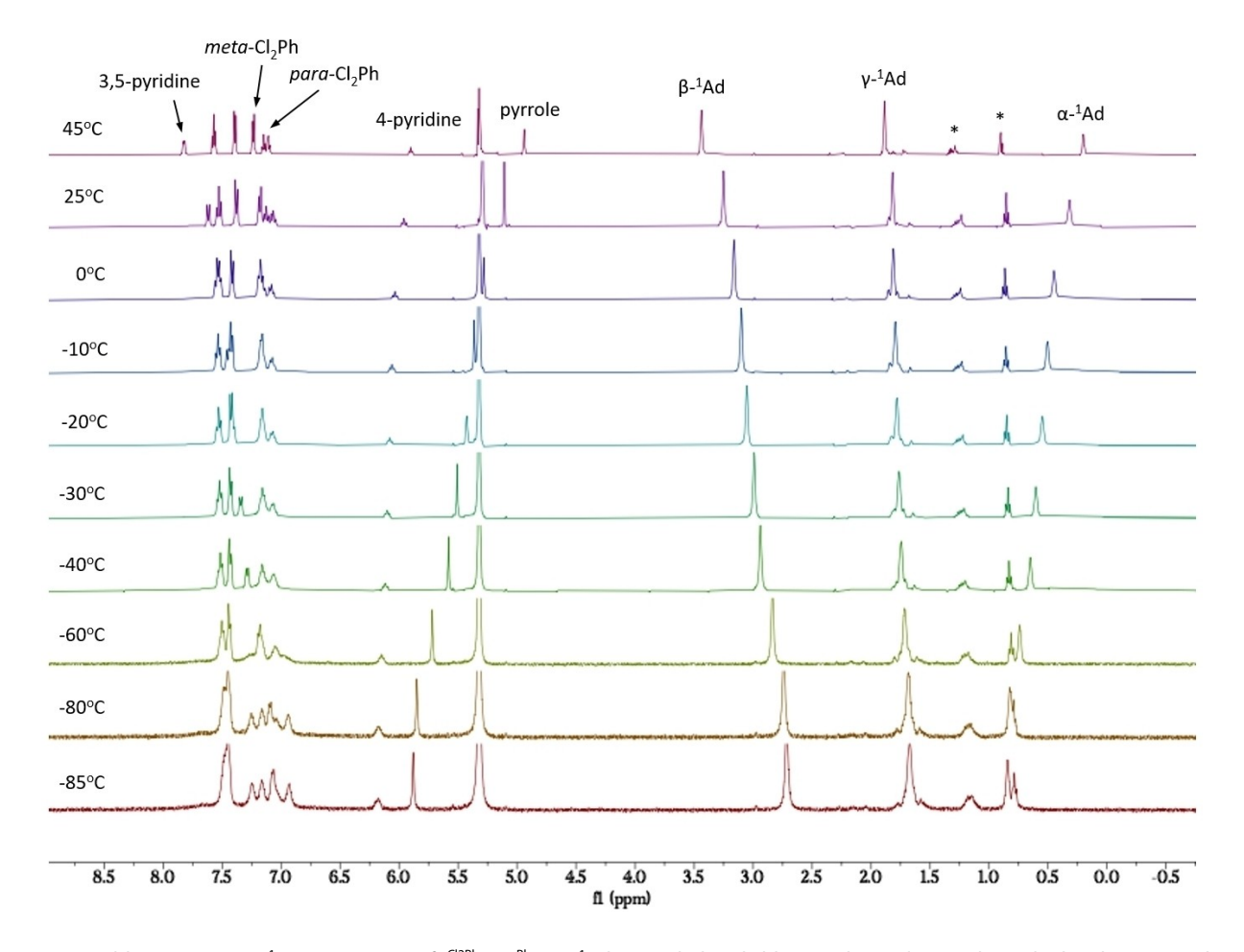


Figure 7. Variable-temperature ¹H NMR spectra of ($^{C12Ph}PDP^{Ph}$)Fe(N¹Ad) recorded in dichloromethane- d_2 . Signals marked with an asterisk are due to residual pentane.

protons in the α - and β -positions to the imido nitrogen are observed slightly more downfield (3.28 ppm) and upfield (0.34 ppm), respectively, than expected for typical adamantyl substituents. The VT-NMR spectra shown in Figure 7 highlight the remarkable temperature-dependence of the previously discussed resonances. The observation of chemical shift variations of more than 0.5 ppm in the recorded temperature window is inconsistent with simple diamagnetic behavior or temperature-independent paramagnetism as suggested previously for (tBuPDPtBu)Fe(N1Ad).9 Instead, the data support residual paramagnetism due to thermal population of excited states with S=1 or S=2. This is also consistent with the fact that the protons whose chemical shifts are the most sensitive to temperature changes are the ones most strongly interacting with the metal center, either by conjugation with the PDP π system (pyrrole and pyridine) or their proximity to the imido unit (α - and β -1-adamantyl). In contrast, the signals for the phenyl substituents and the γ-1-adamantyl protons are essentially unaffected by the temperature changes.

Computational studies of (CI2PhPDPPh)Fe(N1Ad). To further analyze the electronic structure of (CI2PhPDPPh)Fe(N1Ad) and explain the unusual NMR behavior, density functional theory (DFT) and complete active-space self-consistent field (CASSCF) calculations were conducted. Similar to our previous investigations for (MesPDPPh)Fe(NR), full-molecule geometry optimizations at the B3LYP level were conducted first (Table S4 - S5). Several different electronic structures were considered by assuming closed-shell, RKS, and open-shell singlet, BS(1,1), configurations to account for the experimentally observed ground state (BS= broken symmetry). Additionally, the lowest energy triplet and quintet states were computed as BS(3,1) and UKS5, respectively. These electronic structures are best described as containing either a low-spin Fe^{IV}-imido or low-spin Fe^{II}-nitrene unit (RKS), a low-spin Fe^{III} ion antiferromagnetically coupled to an imidyl radical (BS(1,1)), an intermediate-spin Fe^{III} ion antiferromagnetically coupled to an imidyl radical (BS(3,1)), or an intermediatespin Fe^{III} ion ferromagnetically coupled to an imidyl radical (UKS5). These electronic structure descriptions are consistent with our previous studies for putative (MesPDPPh)Fe(NR) intermediates.14

Notably, changes in spin state for (CI2PhPDPPh)Fe(N¹Ad) were found to be accompanied by substantial geometric changes best reflected by the $N_{py}\text{-Fe-N}_{imido}$ angle. While both singlet solutions closely reproduce the crystallographic data ($N_{py}\text{-Fe-N}_{imido}$: exp.: 123.1(2)°; BS(1,1): 122.7°; RKS: 119.0°), the triplet and quintet solutions prefer increasingly larger angles ($N_{py}\text{-Fe-N}_{imido}$: BS(3,1): 148.5°; UKS5: 157.9°) resulting in structures closer to a square-planar coordination geometry (for additional structural parameters see Table S4). Overall, the BS(3,1) triplet was found to be the lowest energy solution followed closely by the quintet (+0.96 kcal/mol) and the two singlet states (BS(1,1): +3.72 kcal/mol; RKS: +4.52 kcal/mol).

Based on the well-established difficulties of DFT to accurately model spin-state energetics²⁷ and the discrepancy between the experimentally observed singlet ground state and our DFT results, *ab-initio* CASSCF calculations were investigated. In accordance with guidelines set forth by Pierloot²⁸ and Roos,²⁹

the active space describing the [Fe=N¹Ad]²⁺ unit in (Cl2PhPDPPh) Fe(N¹Ad) included all five Fe 3d-orbitals, two N¹Ad 2p-orbitals, and one ligand orbital which includes an N¹Ad sp-hybrid. This active space was occupied with 10 electrons, giving rise to an initial CAS(10,8) reference. Full-molecule, state-specific CASSCF calculations with dynamic correlation added via n-electron valence state perturbation theory (NEVPT2) were conducted for each of the three different structures obtained by DFT geometry optimizations for singlet (BS(1,1)), triplet (BS(3,1)), and quintet (UKS5) configurations. This route allows for optimization of the orbital and CI expansion coefficients for each state of interest. The relative energies for each of the nine individual calculations are compared in Figure 8 and predict a diamagnetic singlet state with cis-divacant octahedral geometry as the global minimum, in agreement with experiment. Analysis of the natural orbitals for the singlet state (Figure 9) highlights the highly covalent nature of the Fe= N^1 Ad π -bond. While this covalency renders a definitive computational assignment of the iron oxidation state ambiguous, the electronic structure of (Cl2PhPDPPh)Fe(N1Ad) can be approximated as containing a lowspin Fe^{IV} center with a dianionic imido ligand if a simplified electronic structure assignment is desired. In this limiting description, the four d-electrons of the Fe^{IV} center occupy the d_{xv} and d_{xz} orbitals, consistent with the previous assignment for (tBuPDPtBu)Fe(N1Ad) by Mindiola and coworkers based on DFT calculations.[9]

Interestingly, the relative ordering of the three different spin states changes substantially for the more planar structure (N_{DV}-Fe-N_{imido}: 157.9°), indicating that a paramagnetic triplet state would be the ground state for this geometry. It should be noted that although the CASSCF/NEVPT2 method should in principle give more accurate spin-state energetics for a multiconfigurational molecule like (CI2PhPDPPh)Fe(N1Ad), it has been demonstrated numerous times this is still a formidable challenge.^{30,31} Often times, different states possess different degrees of dynamic correlation (high-spin vs. low-spin) which is not guaranteed to be handled equitably by perturbation theory. A further complication is that the doubleshell effect has not been captured by our CAS(10,8) reference. The inclusion of the 4d (often called 3d') shell in the zeroth-order wavefunction is important to account for radial electron correlation, a phenomenon which is not handled by perturbation theory but has been shown to improve the accuracy of electronic structures and spin-state energetics. [30,32-36] Inclusion of these high-energy orbitals has also proven critical to obtaining more accurate electronic descriptions for other systems with M=E (M=Mn or Fe; E=O or N) multiple bonds. [35,36] Attempts to investigate statespecific CASSCF/NEVPT2 calculations including the Fe 4d orbitals resulted in difficulties with retaining them in the active space (see SI for more details). For this reason, a state-averaged approach using the CAS(10,13) reference was investigated and provided smooth convergence in all cases. While the singlet state in cis-divacant octahedral geometry remains the global energy minimum, the triplet and quintet configurations are substantially lower in energy than the singlet state for the more planar structures (Figure 10). This is perhaps most extreme for

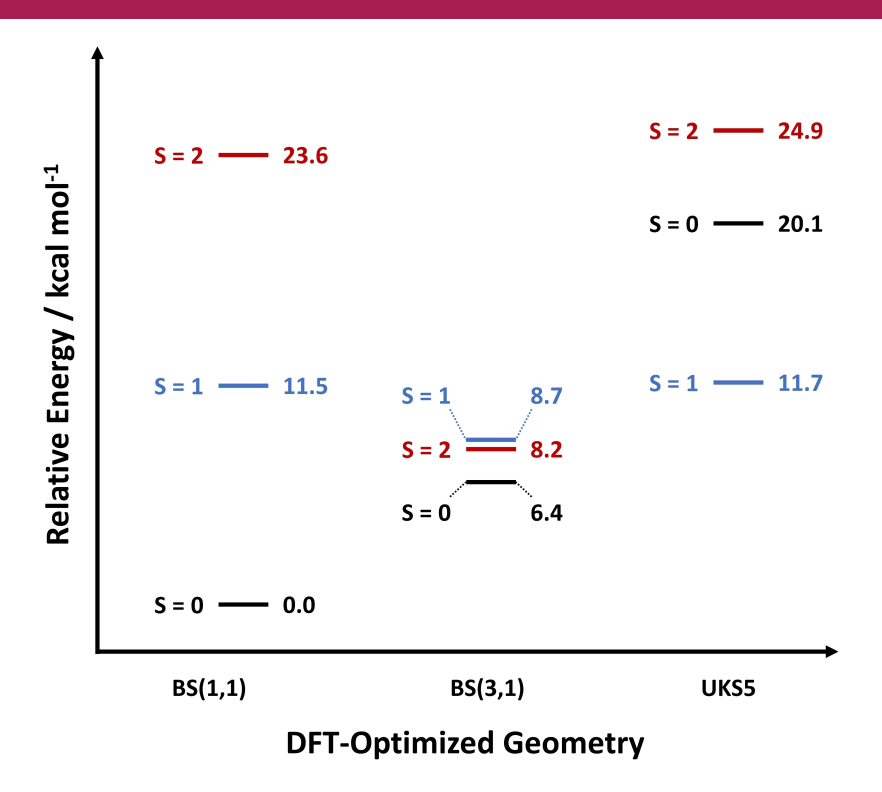


Figure 8. Relative spin-state energetics from state-specific CASSCF/NEVPT2 calculations for (PhCl2PDPPh)Fe(N1Ad) using a CAS(10,8) reference.

the triplet state at the BS(3,1) geometry, which is essentially isoenergetic to the *cis*-divacant octahedral singlet state.

Independent of the CASSCF approach, our calculations suggest that the lowest energy electronic structure for $(^{Cl2Ph}PDP^{Ph})Fe(N^1Ad)$ is a singlet with \emph{cis} -divacant octahedral geometry, as observed experimentally, but that paramagnetic states are favorable for more planar structures. Based on these results, we propose that the unusual magnetic properties observed by VT-NMR spectroscopy are due to rapid interconversion of two C_s-symmetric structures through a wagging motion of the imido ligand rather than rotation of the 2,6-dichlorophenyl substituents (Figure 11). This process involves a square-planar transition state which requires crossing to the lower energy paramagnetic surface(s) at this geometry, introducing small paramagnetic contributions. The involvement of different spin-surfaces during the geometric interconversion is akin to "two-state reactivity", which has been extensively studied computationally to explain the reactivity of high-valent complexes^[37–39] and organometallic iron-oxo iron compounds.[40-42]

Concluding Remarks

The main objective of the present work was the introduction of a new pyridine dipyrrolide ligand with 2,6-dichlorophenyl substituents, [Cl2PhPDPPh]²⁻, as a more robust alternative to previously reported [MesPDPPh]²⁻, which carries mesityl substituents with weak benzylic C–H bonds. The similarities of both ligand frameworks were clearly demonstrated by structural and

spectroscopic comparison of the corresponding five-coordinate iron bis-pyridine adducts, (RPDPPh)Fe(py)2. For the formally fourcoordinate complexes (CI2PhPDPPh)Fe(OEt2) and (CI2PhPDPPh)Fe(thf), introduction of the 2,6-dichlorophenyl groups allows for an additional weak interaction between the iron center and one of the chloro substituents as determined by X-ray crystallography, resulting in a substantial lift of the ether-type ligand out of the plane defined by the pincer ligand. This geometry change compared to the more planar [MesPDPPh]2- analogs is also reflected in the Mössbauer spectroscopic parameters. Despite clear evidence for the Fe-Cl interaction in the solid state, NMR spectroscopic data indicate more flexible structures in solution, which allowed further reactivity of (CI2Ph PDPPh)Fe(thf) with 1adamantyl azide. As hypothesized, [Cl2PhPDPPh]2- provides a more inert ligand framework with respect to intramolecular C-H activation and allowed the isolation of a high-valent Fe^{IV}imido complex, (CI2PhPDPPh)Fe(N1Ad). The electronic structure of cis-divacant octahedral (Cl2PhPDPPh)Fe(N1Ad) was investigated by DFT and CASSCF/NEVPT2 calculations to elucidate the temperature-dependence of the chemical shifts observed by ¹H NMR spectroscopy, which indicated occupation of low-lying paramagnetic excited states. These computational studies revealed energetically close-lying singlet, triplet, and quintet states consistent with the unusual magnetic behavior observed spectroscopically. The CASSCF/NEVPT2 approach successfully reproduced the experimental singlet ground state for (CI2PhPDPPh)Fe(N1Ad) and further predicted that paramagnetic ground states for more planar structures may be accessible at room temperature in solution.

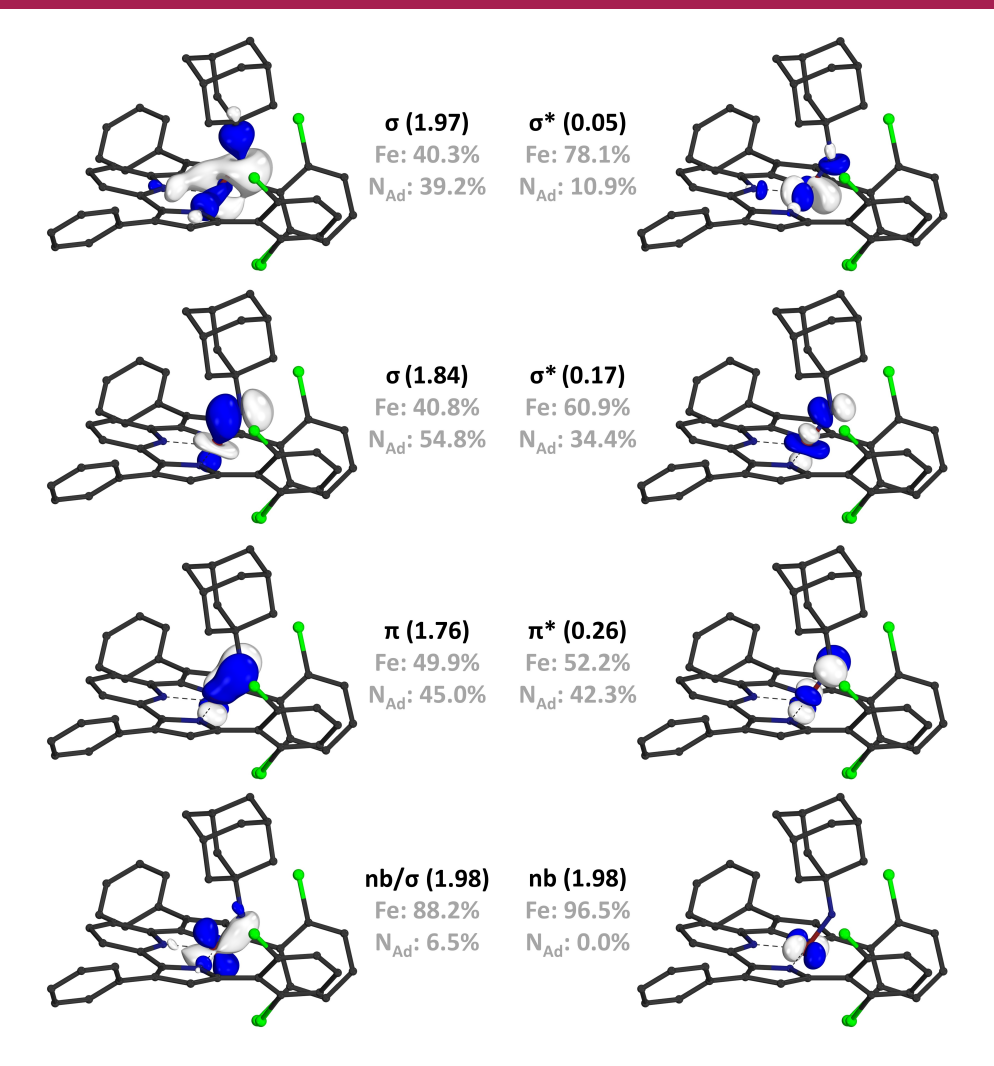


Figure 9. Natural orbitals for the lowest singlet state of $(^{PhCI2}PDP^{Ph})Fe(N^1Ad)$ at the BS(1,1) optimized geometry. The orbital natures and occupation numbers are provided along with atomic contributions for Fe and the N^1Ad substituent.

Experimental Details

General Considerations. All air- and moisture-sensitive manipulations were carried out using standard high vacuum line. Schlenk, or cannula techniques or in an MBraun inert atmosphere drybox containing an atmosphere of purified nitrogen. All solids were dried under high vacuum in order to bring into the glovebox. Solvents for air- and moisture-sensitive manipulations were dried and deoxygenated using a Glass Contour Solvent Purification System and stored over 4 Å molecular sieves. Deuterated solvents for NMR spectroscopy were purchased from Cambridge Isotope Laboratories and distilled from sodium metal (C₆D₆) or CaH₂ (CD₂Cl₂). 1-(2,6dichlorophenyl)-3-phenyl-2-propen-1-one was prepared following a literature procedure.43 1-Adamantyl azide was purchased from Sigma-Aldrich, dried under high vacuum, and recrystallized from anhydrous pentane at $-35\,^{\circ}\text{C}$ prior to use. All remaining chemicals were purchased from commercial sources (Fisher Scientific, VWR, Sigma Aldrich) and used without further purification.

Safety Considerations. Organic azides are known energetic materials that may decompose violently via explosion upon input of energy from external sources (heat, light, pressure). While we did not encounter any problems or dangerous situations during the course of this study, all experiments involving 1-adamantyl azide

were performed on small scale with less than 100 mg of azide material. 1-Adamantyl azide was stored in the dark at $-35\,^{\circ}$ C in the drybox. All iron complexes are thermally stable upon heating to $45\,^{\circ}$ C in benzene- d_6 or dichloromethane- d_2 . No experiments at higher temperatures were performed.

Preparation of 4-(2,6-dichlorophenyl)-1-{6-[4-(2,6-dichlorophenyl)-4oxo-2-phenylbutanoyl]pyridin-2-yl}-2-phenylbutane-1,4-dione. In a 250 ml Schlenk flask, 595 mg (4.40 mmol) of 2,6-pyridinecarboxaldehyde, 2.5 grams (9.02 mmol) of 1-(2,6-dichlorophenyl)-3-phenyl-2propen-1-one, and 890 mg (3.30 mmol) of 3-benzyl-5-(2-hydroxyethyl)-4-methylthiazolium chloride were combined with a magnetic stirrer and 15 mL of absolute ethanol. A reflux condenser was affixed to the flask and the apparatus was attached to a Schlenk line and purged for 5 minutes with argon. The apparatus was then degassed, and again purged with argon. This procedure was repeated four additional times. In a separate flask, 317 mg (3.30 mmol) of sodium tert-butoxide was dissolved in 5 mL of absolute ethanol. The sodium tert-butoxide solution was added to the Schlenk flask under a heavy flow of argon. An immediate color change to dark-brown was observed. The mixture was then brought to a gentle reflux, which was maintained for 12 hrs. The resulting tan precipitate was isolated on a medium porosity frit, washed with three 10 mL aliquots of cold ethanol, and dried under vacuum. Yield: 2.28 grams (3.31 mmol), 75%. ¹H NMR (400 MHz,

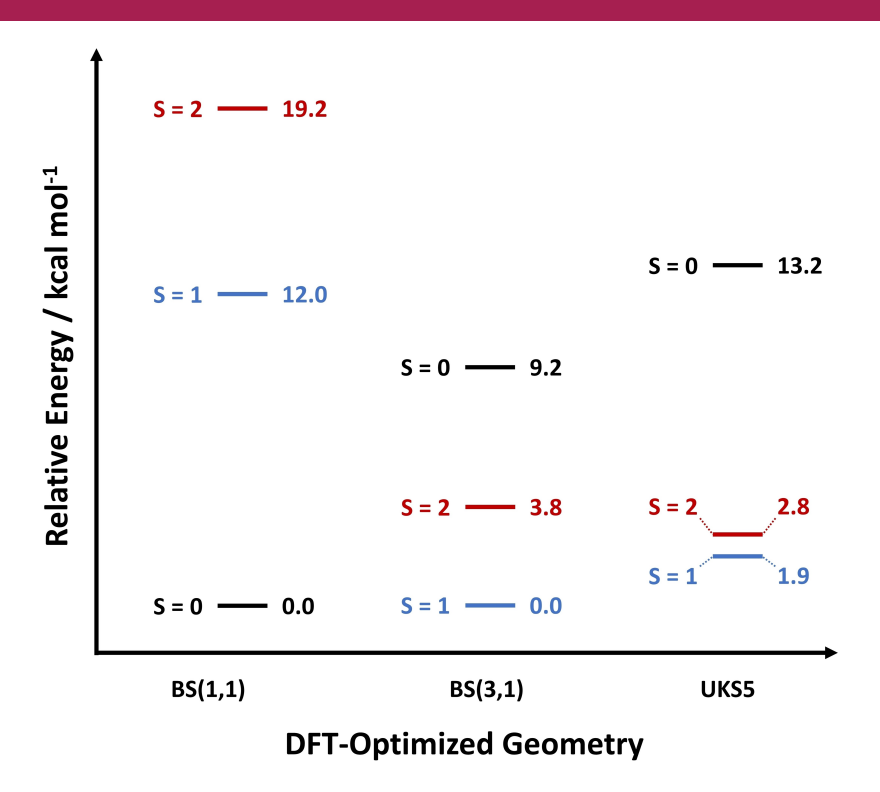
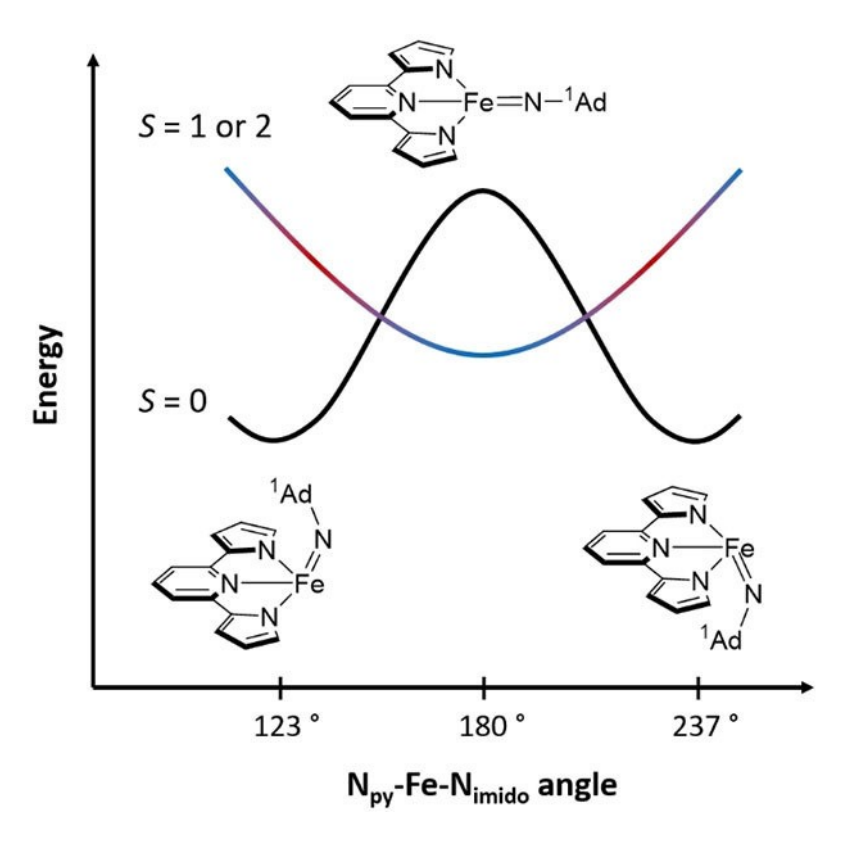


Figure 10. Relative spin-state energetics from state-averaged CASSCF/NEVPT2 calculations on (PhCl2PDPPh)Fe(N1Ad) using a CAS(10,13) reference.



 $\textbf{Figure 11.} \ \ \textbf{Qualitative depiction of the proposed interconversion of two isoenergetic } C_s\text{-symmetric conformations for } (^{Cl2Ph}PDP^{Ph})Fe(N^1Ad)$ involving multiple spin states.

CDCl₃) δ 8.21 (d, J=7.8 Hz, 2H), 7.95 – 7.87 (m, 1H), 7.66 – 7.58 (d, J=7.2 Hz, 4H), 7.36 – 7.27 (m, 10H), 7.19 (t, J=7.4 Hz, 2H), 6.34 (dd, J=10.1, 3.7 Hz, 2H), 4.17 (dd, J=19.0, 10.1 Hz, 2H), 3.46 (dd, J=19.0, 3.7 Hz, 2H). 13 C NMR (101 MHz, CDCl₃) δ 45.46, 47.27, 126.46, 127.64, 128.26, 129.13, 129.20, 130.78, 137.08, 138.29, 139.21, 151.27, 198.24, 200.23, one resonance was not detected. HRMS (ESI) calcd for $C_{37}H_{26}N_1O_4Cl_4^+$ [M+H] $^+$ 688.0610 m/z. Found 688.0620 m/z.

Preparation of 2,6-Bis(5-(2,6-dichlorophenyl)-3-phenyl-1H-pyrrol-2yl)-pyridine, H₂CI2PhPDP^{Ph}. A 250 mL round bottom flask was loaded with 2.28 grams (3.31 mmol) of 1,1'-(2,6-pyridinediyl)bis[2-phenyl-4-(2.6-dichlorophenyl)]-1.4-butanedione, 3.00 grams (38.9 mmol, 11.75 eg) of ammonium acetate, and a magnetic stirrer. 25 mL of glacial acetic acid was added to the mixture. A condenser was affixed to the flask and the mixture was brought to a vigorous reflux, which was maintained for approximately 48 hrs. The resulting yellow precipitate was then isolated via vacuum filtration and washed with three 15 mL aliquots of cold ethanol. The solid was collected and extracted into dichloromethane and passed through a plug of basic alumina. Removal of the solvent in vacuo afforded a light yellow powder. Yield: 1.45 g (2.22 mmol), 67 %. Single crystals suitable for study via X-ray crystallographic analysis were obtained from a concentrated dimethyl sulfoxide solution of the compound. ^{1}H NMR (400 MHz, DMSO- d_{6}) δ 11.54 (d, J=2.5 Hz, 2H, pyrrole-NH), 7.62 (d, J=8.2 Hz, 4H, ArH), 7.43 (m, 10H, ArH), 7.31 (m, 3H, ArH), 6.94 (d, J=8.0 Hz, 2H, ArH), 6.30 (d, J=2.9 Hz, 2H, pyrrole-CH). ¹³C NMR (101 MHz, DMSO- d_6) δ 113.55, 116.43, 124.45, 126.20, 126.64, 127.16, 128.60, 128.66, 129.03, 130.83, 131.44, 135.84, 136.39, 136.76, 149.69. HRMS (ESI) calcd for C₃₇H₂₄N₃⁺ $[M+H]^+$ 650.0719 m/z. Found 650.0767 m/z.

Preparation of (CI2PhPDPPh)Fe(py)2. To a 20 mL vial equipped with a magnetic stirrer was added 153 mg (0.345 mmol) of Fe(Cl)₂(py)₄ and 15 mL of pentane. Vigorous stirring afforded a yellow suspension. In a separate vial 65 mg (0.690 mmol, 2.0 eq.) of (trimethylsilyl) methyllithium was dissolved in 5 mL of pentane. The (trimethylsilyl) methyllithium solution was added to the suspension of Fe(Cl)₂(py)₄, inducing a rapid color change to dark-purple. The reaction mixture was allowed to stir for two hours, at which time it was filtered through a pad of Celite supported on a glass microfiber filter into a round bottom flask. In a separate vial, 225 mg (0.345 mmol) of $H_2^{Cl2Ph}PDP^{Ph}$ was suspended in 5 mL of toluene and 10 mL of pentane. The ligand suspension was added dropwise to the stirring solution of Fe(Ns)₂(py)₂, inducing a color change to yellow-orange within minutes accompanied by precipitation of an orange solid. After one hour, the precipitate was collected on a medium porosity glass frit and washed with three 5 mL aliquots of pentane, and dried in vacuo. Yield: 167 mg (0.193 mmol), 56%. Single crystals of the compound were grown from slow evaporation of a dichloromethane solution over 36 hrs. $\mu_{\rm eff}$ = 4.7 $\mu_{\rm B}$ (295 K, magnetic susceptibility balance). ¹H NMR (400 MHz, benzene- d_6) δ 110.77 (broad singlet, 4H), 83.19 (singlet, 2H), 76.19 (singlet, 2H), 38.08 (singlet, 4H), 24.23 (singlet, 4-pyridine-H, 1H), 9.41 (singlet, 4H), 7.48-8.08 (overlapping broad singlets, 6H), 7.25 (singlet, 2H), 7.04 (singlet, 4H), 5.31 (singlet, 2H). Anal. Calcd for (CI2Ph PDPPh) Fe(py)₂, C₄₇H₃₁Cl₄FeN₅: C, 65.38; H, 3.62; N, 8.11. Found: C, 64.93; H, 3.98; N. 7.80.

Preparation of (C12PhPDPPh)Fe(OEt₂). In the glovebox, 18 mg (0.048 mmol) of Fe[N(SiMe₃)₂]₂ was loaded in a 20 mL vial equipped with a magnetic stirrer and 5 mL of Et₂O was added. Vigorous stirring afforded a homogeneous pale green solution. In a separate vial, a 3 mL solution of 26 mg (0.040 mmol, 0.833 eq.) of $H_2^{C12Ph}PDP^{Ph}$ in diethyl ether was prepared. The solution of $H_2^{C12Ph}PDP^{Ph}$ was added to the solution of the iron complex dropwise over the course of 15 minutes. A color change from green to orange/red was noted and the mixture was allowed to stir at room temperature overnight. Removal of volatiles *in vacuo* afforded an orange/red powder which was analyzed via 1H NMR spectroscopy in benzene- d_6 . The resulting spectrum indicated complete consumption of $H_2^{C12Ph}PDP^{Ph}$ with

concomitant formation of a mixture of paramagnetic species. Single crystals grown from a concentrated toluene solution of the crude layered with diethyl ether @ $-35\,^{\circ}\text{C}$ were identified as $(^{\text{Cl2Ph}}\text{PDPPh})$ Fe(OEt_2) by X-ray crystallography. To date, the title compound has proved challenging to isolate on a preparative scale, thus precluding its unambiguous assignment by ^{1}H NMR spectroscopy and elemental analysis.

Preparation of (C12PhPDPPh)Fe(thf). In the glovebox, 500 mg (0.768 mmol) of H₂Cl2PhPDPPh and 10 mL of THF were loaded in a 100 mL flask equipped with a magnetic stirrer. In a separate vial, 265 mg (1.58 mmol) of LiHMDS was combined with 3 mL of THF. While vigorously stirring, the solution of LiHMDS was added to the solution of H₂Cl2PhPDPPh, resulting in an immediate color change from tan to a brilliant fluorescent yellow. The mixture was stirred for approximately two hours. In a separate 250 mL round bottom flask, 97 mg (0.765 mmol) of FeCl₂, 20 mL of THF, and a magnetic stirrer were combined. While vigorously stirring, the solution of deprotonated ligand was added to the THF slurry of FeCl₂, resulting in an immediate color change to an intense dark-red. After 12 hours, the mixture was homogenous and the volume of solvent was reduced to approximately 3 mL. 75 mL of diethyl ether was added, and immediate precipitation of a bright orange solid was observed. The resulting solid was isolated on a medium porosity glass frit and dried in vacuo. The solid was transferred to a 20 mL vial and combined with 5 mL of toluene, 10 mL of pentane, and a magnetic stirrer. Rapid stirring of the mixture induced precipitation of lithium chloride. The suspension was then filtered over a medium porosity frit containing a one-inch pad of Celite. The red compound was washed from the Celite first with toluene, and then with dichloromethane, until all washings were clear. Removal of solvent in vacuo, followed by trituration with pentane afforded the title compound as an orange-red powder, which could be recrystallized from a concentrated dichloromethane solution layered with pentane at -35 °C. Yield: 445 mg (0.572 mmol), 74%. $\mu_{\rm eff}$ = 5.1 $\mu_{\rm R}$ (295 K, magnetic susceptibility balance). ¹H NMR (400 MHz, benzene- d_6) δ 106.09 (singlet, 2H), 97.77 (singlet, 2H), 16.53 (broad singlet, 4H), 13.45 (singlet, 4H), 12.23 (singlet, 4H), 11.91 (singlet, 4H), 9.76 (singlet, 2H), 7.99 (singlet, 4H), 0.33 (1H, 4-pyridine-H). One resonance could not be located. Anal. Calcd for (C12PhPDPPh)Fe(thf), C41H29Cl4FeN3O: C, 63.35; H, 3.76; N, 5.41. Found: C, 62.64; H, 3.75; N, 5.23. The low carbon value observed in the CHN analysis suggests that despite multiple extractions of the compound via hydrocarbon solvents 1/3 eq. of LiCl is still present in (CI2PhPDPPh)Fe(thf)•1/3(LiCl), Anal. Calcd for sample. C₄₁H₂₉Cl_{4,33}FeLi_{0,33}N₃O: C: 62.23; H: 3.69; N: 5.31. Found: 62.64; H, 3.75; N, 5.23. Single crystals suitable for an X-ray study were grown from diffusion of pentane into a concentrated benzene solution of the title compound at room temperature.

Preparation of (Clapher PDPPh)Fe(thf)₂. 15 mg of (Clapher PDPPh)Fe(thf) was weighed into a one dram vial. A 500 μ L aliquot of THF was added, resulting in complete dissolution of the compound. The resulting mixture was filtered into a J. Young NMR tube, affording a homogeneous orange solution. On a high-vacuum line, the THF solvent was removed. After two hours, THF-d₈ was vacuum transferred onto the sample, again affording a homogeneous orange solution. Analysis by ¹H NMR spectroscopy demonstrated quantitative conversion to (CI2PhPDPPh)Fe(thf)2, as demonstrated by the downfield shift of the resonance corresponding to the 4-pyridine proton. The J. Young tube was returned to the glovebox and one drop of pentane was added to the sample as a secondary internal standard. A ¹H NMR spectrum was again acquired, with the resonances corresponding to $(^{Cl2Ph}PDP^{Ph})Fe(thf)_2$ unchanged. ¹H NMR (400 MHz, THF- d_8) δ 85.38 (singlet, 2H), 65.88 (singlet, 2H), 22.15 (singlet, 4-pyridine-H, 1H), 8.02 (singlet, 4H), 7.08 (singlet, 4H), 6.86 (singlet, 2H), 6.41 (singlet, 4H), 5.97 (singlet, 2H). Note, resonances for the THF ligands were not observed due to rapid exchange with THF-d₈. Single crystals suitable for an X- ray study were grown from a THF/diethyl ether solution of the compound at $-35\,^{\circ}\text{C}$.

Preparation of (Cl2PhPDPPh)Fe(N1Ad). In the glovebox, a thick-walled glass vessel was charged with 50 mg (0.064 mmol) of (CI2PhPDPPh)Fe(thf) and 10 mL of dichloromethane, resulting in a clear dark-red solution. A solution of 13 mg (0.074 mmol) of 1-adamantyl azide in 5 mL of dichloromethane was added and the vessel was sealed with a Teflon screw cap. The reaction mixture was heated to 40-45 °C for 4 h using an oil bath, resulting in a color change to dark brown. The vessel was then returned to the glovebox, and the brown solution was concentrated in vacuo to a volume of approximately 2-3 mL. A large excess of pentane (20-30 mL) was added, providing a dark brown precipitate over the course of 20 min. The solid was collected on a medium porosity glass frit, washed multiple times with pentane, and dried in vacuo, yielding 44 mg (0.052 mmol), 81% of the target complex. ¹H NMR (400 MHz, dichloromethane- d_2 , 25 °C) δ 7.62 (d, J=7.8 Hz, 2H, 3-pyridine-*H*), 7.53 (t, J=7.4 Hz, 4H, *m*-Ph*H*), 7.38 (d, J=7.2 Hz, 4H, o-PhH), 7.18 (d, J = 8.0 Hz, 4H, m-Cl₂PhH), 7.12 (t, J = 7.2 Hz, 2H, p-PhH), 7.07 (t, J=7.8 Hz, 2H, p-Cl₂PhH), 5.96 (t, J=7.6 Hz, 1H, 4pyridine-H), 5.11 (s, 2H, pyrrole-H), 3.25 (broad s, 6H, β-adamantyl-H), 1.82 (broad s, 6H, γ -adamantyl-H), 0.32 (broad s, 3H, α -adamantyl-H). 13 C NMR (101 MHz, dichloromethane- d_2 , 25 °C) δ 168.68, 154.89, 148.10, 137.44, 135.48, 133.55, 130.66, 129.09, 128.71, 128.05, 127.82, 126.95, 116.66, 106.31, 40.43, 36. 86, 36.75, 36.24, 28.96, 28.00. Single crystals of (Cl2PhPDPPh)Fe(N1Ad) suitable for single-crystal X-ray diffraction were obtained by slow evaporation of a diethyl ether solution at -35°C.

Physical Measurements. ¹H and ¹³C {¹H} NMR spectra were acquired at 25 °C on a Varian INOVA Unity 600 MHz spectrometer equipped with a 5 mm inverse broadband PFG probe, on an Agilent 400 MHz DD2 spectrometer equipped with a 5 mm One NMR probe, or a JNM-ECZ400S/L1 spectrometer equipped with a 5 mm ROYAL NMR probe. All chemical shifts are reported relative to SiMe₄ using ¹H (residual) chemical shifts of the solvent as a secondary standard. Elemental analyses were performed at Robertson Microlit Laboratories, Inc., in Ledgewood, NJ. Room temperature magnetic susceptibility measurements were performed with a Johnson Matthey Mark 1 instrument that was calibrated with HgCo(SCN)₄. Zero field ⁵⁷Fe Mössbauer spectra were collected on a SEE Co. Mössbauer spectrometer (MS4) with a ⁵⁷Co/Rh radiation source at 80 K in constant acceleration mode. The temperature in the sample chamber was controlled by a Janis Research Co. CCS-850 He/N $_2$ cryostat within an accuracy of ± 0.3 K. The data were calibrated relative to α -iron at 298 K. The fitting procedure to extract quantitative spectral parameters uses a leastsquares Lorentzian fitting method implemented in the WMOSS software developed by SEE Co.

X-Ray Crystallography. Single crystals suitable for X-ray diffraction were coated with polyisobutylene oil (Sigma-Aldrich) in a drybox, mounted on a nylon loop, and then quickly transferred to the goniometer head of a Bruker AXS D8 Venture fixed-chi X-ray diffractometer equipped with a Triumph monochromator, a Mo $K\alpha$ radiation source (λ =0.71073 Å), and a PHOTON 100 CMOS detector. The samples were cooled to 100 K with an Oxford Cryostream 700 system and optically aligned. The APEX3 software program (version 2016.9-0)44 was used for diffractometer control, preliminary frame scans, indexing, orientation matrix calculations, least-squares refinement of cell parameters, and the data collection. Three sets of 12 frames each were collected using the omega scan method with a 10 s exposure time. Integration of these frames followed by reflection indexing and least-squares refinement produced a crystal orientation matrix for the crystal lattice that was used for the structural analysis. The data collection strategy was optimized for completeness and redundancy using the Bruker COSMO software suite. The space group was identified, and the data were processed using the Bruker SAINT+ program and corrected for absorption using SADABS. The structures were solved using direct methods (SHELXS) completed by subsequent Fourier synthesis and refined by full-matrix least-squares procedures using the programs provided by SHELXL-2014.⁴⁵ Further collection and refinement detail can be found in the Supporting Information.

Computational Methods. All calculations were performed using the ORCA quantum chemical program package v4.2.1. [46,47] Geometry optimizations used the crystallographically determined structure as the starting point and employed the B3LYP density functional [48] with tight self-consistent field (SCF) and geometry convergence criteria. The calculations were accelerated by using RIJCOSX [49] (resolution of identity for the Coulomb term and a chain of spheres algorithm for exact exchange) and noncovalent interactions were considered via atom-pairwise dispersion corrections with Becke-Johnson (D3BJ) damping. [50,51] The def2-TZVP basis set was used on iron and all atoms in its first coordination sphere while the smaller def2-SVP basis set was used for all other atoms. [52] All auxiliary basis sets in the DFT calculations were generated via the autoaux procedure. [53]

All complete-active-space self-consistent field (CASSCF)^[54] studies were performed as single-point calculations on the structure of interest. Dynamic electron correlation was recovered via N-electron valence state perturbation theory in the domain-based local pair natural orbital framework (DLPNO-NEVPT2). [55] Like in the DFT calculations, the RIJCOSX approximation was used in conjunction with tight SCF convergence criteria (E_{tol} was modified to 10^{-7} E_h). The same primary basis sets were used as in the DFT calculations. For computational efficiency, the universal def2/J Coulomb-fitting auxiliary basis set [56] was used in conjunction with the appropriate correlation-fitting auxiliaries (i.e. def2-SVP/C or def2-TZVP/C). [57] The truncation of the 4-RDM term in the NEVPT2 calculations was tightened from the default 10^{-10} to 10^{-13} to further protect against intruder states.

Obtaining the desired CAS(10,8) wavefunction was achieved by using either Quasi-restricted orbitals (QROs) from a DFT calculation or a CASCI wavefunction as initial guess. Convergence of an initial CAS(8,7) calculation accompanied with the PMOs option in ORCA allowed identification of the desired sigma-bonding orbital. Rotation of this orbital into the CAS(10,8) active space provided smooth convergence.

Supporting Information

Spectroscopic and crystallographic data, and additional computational details. The Supporting Information is available free of charge.

Acknowledgements

West Virginia University is acknowledged for financial support. D.C.L. and C.M. thank the National Science Foundation (CHE-1752738) for additional support. This work used X-ray crystallography (CHE-1336071) and NMR (CHE-1228336) instrumentation funded by the National Science Foundation. The WVU High Performance Computing facilities are funded by the National Science Foundation EPSCOR Research Infrastructure Improvement Cooperative Agreement #1003907, the state of West Virginia (WVEPSCOR via the Higher Education Policy Commission), the WVU Research Corporation, and faculty investments. The authors thank Prof. Paul J. Chirik (Princeton University) for providing access to his group's Mössbauer spectrometer. B.M.H.

would like to thank Sherman Adams (WVU) for construction of the specialty glassware utilized in this study.

Conflict of Interest

The authors declare no conflict of interest.

- [1] N. Komine, R. W. Buell, C.-H. Chen, A. K. Hui, M. Pink, K. G. Caulton, Inorg. Chem. 2014, 53, 1361-1369.
- [2] S. Yadav, C. Dash, Tetrahedron 2020, 76, 131350.
- [3] Y. Zhang, J. L. Petersen, C. Milsmann, J. Am. Chem. Soc. 2016, 138, 13115-13118.
- [4] Y. Zhang, T. S. Lee, J. L. Petersen, C. Milsmann, J. Am. Chem. Soc. 2018, 140, 5934-5947.
- [5] Y. Zhang, D. C. Leary, A. M. Belldina, J. L. Petersen, C. Milsmann, Inorg. Chem. 2020, 59, 14716-14730.
- [6] Y. Zhang, T. S. Lee, J. M. Favale, J. L. Petersen, G. D. Scholes, F. N. Castellano, C. Milsmann, Nat. Chem. 2020, 12, 345.
- [7] A. S. Gowda, J. L. Petersen, C. Milsmann, Inorg. Chem. 2018, 57,
- [8] Z. R. Turner, Inorg. Chem. 2019, 58, 14212-14227.
- [9] K. Searles, S. Fortier, M. M. Khusniyarov, P. J. Carroll, J. Sutter, K. Meyer, D. J. Mindiola, K. G. Caulton, Angew. Chem. Int. Ed. 2014, 53, 14139-14143.
- [10] D. Sorsche, M. E. Miehlich, E. M. Zolnhofer, P. J. Carroll, K. Meyer, D. J. Mindiola, Inorg. Chem. 2018, 57, 11552-11559.
- [11] D. Sorsche, M. E. Miehlich, K. Searles, G. Gouget, E. M. Zolnhofer, S. Fortier, C. H. Chen, M. Gau, P. J. Carroll, C. B. Murray, et al., J. Am. Chem. Soc. 2020, 142, 8147-8159.
- [12] L. N. Grant, M. E. Carroll, P. J. Carroll, D. J. Mindiola, Inorg. Chem. 2016, 55, 7997-8002.
- [13] B. M. Hakey, J. M. Darmon, Y. Zhang, J. L. Petersen, C. Milsmann, Inorg. Chem. 2019, 58, 1252-1266.
- [14] B. M. Hakey, J. M. Darmon, N. G. Akhmedov, J. L. Petersen, C. Milsmann, Inorg. Chem. 2019, 58, 11028-11042.
- [15] G. Poignant, S. Nlate, V. Guerchais, A. J. Edwards, P. R. Raithby, Organometallics 1997, 16, 124-132.
- [16] X. Wang, Z. Mo, J. Xiao, L. Deng, *Inorg. Chem.* **2013**, *52*, 59–65.
- [17] M. Bastürkmen, D. Kisakürek, W. Driessen, S. Gorter, J. Reedijk, Inorganica Chim. Acta 1998, 271, 19-23.
- [18] J. A. Davis, C. P. Davie, D. B. Sable, W. H. Armstrong, Chem. Commun. 1998, 670, 1649-1650.
- [19] A. Facchinetti, N. Marsich, A. Camus, F. Ugozzoli, C. Massera, A. M. Manotti Lanfredi, Inorganica Chim. Acta 2001, 324, 162-
- [20] P. J. Alonso, J. Forniés, M. A. García-Monforte, A. Martín, B. Menjón, C. Rillo, J. Organomet. Chem. 2007, 692, 3236-3247.
- [21] O. Hietsoi, C. Dubceac, A. S. Filatov, M. A. Petrukhina, Chem. Commun. 2011, 47, 6939-6941.
- [22] A. G. Bakhoda, S. Wiese, C. Greene, B. C. Figula, J. A. Bertke, T. H. Warren, Organometallics 2020, 39, 1710–1718.
- [23] A. Friedrich, J. Eyselein, J. Langer, S. Harder, Organometallics 2021, 40, 448-457.
- [24] M. G. Clark, G. M. Bancroft, A. J. Stone, J. Chem. Phys. 1967, 47, 4250-4261.
- [25] D. Pinkert, M. Keck, S. G. Tabrizi, C. Herwig, F. Beckmann, B. Braun-Cula, M. Kaupp, C. Limberg, Chem. Commun. 2017, 53, 8081-8084.

- [26] M. E. Pascualini, N. V. Di Russo, A. E. Thuiis, A. Ozarowski, S. A. Stoian, K. A. Abboud, G. Christou, A. S. Veige, Chem. Sci. 2015, 6, 608-612.
- [27] S. Ye, F. Neese, Inorg. Chem. 2010, 49, 772-774.
- [28] K. Pierloot, Mol. Phys. 2003, 101, 2083-2094.
- [29] V. Veryazov, P. Å. Malmqvist, B. O. Roos, Int. J. Quantum Chem. 2011, 111, 3329-3338.
- [30] S. E. Neale, D. A. Pantazis, S. A. Macgregor, Dalton Trans. 2020, 49, 6478-6487.
- [31] B. M. Flöser, Y. Guo, C. Riplinger, F. Tuczek, F. Neese, J. Chem. Theory Comput. 2020, 16, 2224-2235.
- [32] K. Pierloot, Int. J. Quantum Chem. 2011, 111, 3291–3301.
- [33] Q. M. Phung, S. Vancoillie, K. Pierloot, J. Chem. Theory Comput. **2012**, *8*, 883–892.
- [34] G. Drabik, J. Szklarzewicz, M. Radoń, Phys. Chem. Chem. Phys. 2021, 23, 151-172.
- [35] S. A. Venturinelli Jannuzzi, Q. M. Phung, A. Domingo, A. L. B. Formiga, K. Pierloot, Inorg. Chem. 2016, 55, 5168-5179.
- [36] H. C. Chang, B. Mondal, H. Fang, F. Neese, E. Bill, S. Ye, J. Am. Chem. Soc. 2019, 141, 2421-2434.
- [37] S. Shaik, D. Kumar, S. P. de Visser, A. Altun, W. Thiel, Chem. Rev. 2005, 105, 2279-2328.
- [38] S. Shaik, H. Hirao, D. Kumar, Acc. Chem. Res. 2007, 40, 532-542.
- [39] S. Shaik, S. Cohen, Y. Wang, H. Chen, D. Kumar, W. Thiel, Chem. Rev. 2010, 110, 949-1017.
- [40] Y. Sun, H. Tang, K. Chen, L. Hu, J. Yao, S. Shaik, H. Chen, J. Am. Chem. Soc. 2016, 138, 3715-3730.
- [41] L. Hu, H. Chen, J. Am. Chem. Soc. 2017, 139, 15564-15567.
- [42] S. A. Lutz, A. K. Hickey, Y. Gao, C. H. Chen, J. M. Smith, J. Am. Chem. Soc. 2020, 142, 15527-15535.
- [43] T. P. Robinson, R. B. Hubbard IV, T. J. Ehlers, J. L. Arbiser, D. J. Goldsmith, J. P. Bowen, Bioorganic Med. Chem. 2005, 13, 4007-
- [44] APEX3 Is a Bruker AXS Crystallographic Software Package for Single Crystal Data Collection, Reduction and Preparation.
- [45] G. M. Sheldrick, SHELXL-2014, Crystallographic software package, Bruker AXS, Inc., Madison, Wisconsin, USA.
- [46] F. Neese, Wiley Interdiscip. Rev. Comput. Mol. Sci. 2012, 2, 73-
- [47] F. Neese, Wiley Interdiscip. Rev. Comput. Mol. Sci. 2018, 8, 1327.
- [48] C. Lee, W. Yang, R. G. Parr, Phys. Rev. B 1988, 37, 785-789.
- [49] F. Neese, F. Wennmohs, A. Hansen, U. Becker, Chem. Phys. 2009. 356. 98-109.
- [50] S. Grimme, J. Antony, S. Ehrlich, H. Krieg, J. Chem. Phys. 2010, 132, 154104.
- [51] S. Grimme, S. Ehrlich, L. Goerigk, J. Comput. Chem. 2011, 32, 1456-1465
- [52] F. Weigend, R. Ahlrichs, Phys. Chem. Chem. Phys. 2005, 7, 3297-3305.
- [53] G. L. Stoychev, A. A. Auer, F. Neese, J. Chem. Theory Comput. 2017, 13, 554-562.
- [54] B. O. Roos, P. R. Taylor, P. E. M. Sigbahn, Chem. Phys. 1980, 48, 157-173.
- [55] Y. Guo, K. Sivalingam, E. F. Valeev, F. Neese, J. Chem. Phys. **2016**, *144*, 094111.
- [56] F. Weigend, Phys. Chem. Chem. Phys. 2006, 8, 1057-1065.
- [57] A. Hellweg, C. Hättig, S. Höfener, W. Klopper, Theor. Chem. Acc. **2007**, 117, 587-597.

Manuscript received: April 1, 2021 Revised manuscript received: June 4, 2021